JACS
JOURNAL OF THE AMERICAN CHEMICAL SOCIETY

Article

pubs.acs.org/JACS

A Versatile Approach to Organic Photovoltaics Evaluation Using White Light Pulse and Microwave Conductivity

Akinori Saeki,*[,†,‡] Saya Yoshikawa,[†] Masashi Tsuji,[†] Yoshiko Koizumi,[†,§] Marina Ide,[†] Chakkooth Vijayakumar,[†] and Shu Seki[†]

[†]Department of Applied Chemistry, Graduate School of Engineering, Osaka University, 2-1 Yamadaoka, Suita, Osaka 565-0871, Japan
[‡]PRESTO, Japan Science and Technology Agency (JST), 4-1-8 Honcho Kawaguchi, Saitama 332-0012, Japan
[§]RIKEN Advanced Science Institute, 2-1 Hirosawa, Wako, Saitama 351-0198, Japan

Supporting Information

ABSTRACT: State-of-the-art low band gap conjugated polymers have been investigated for application in organic photovoltaic cells (OPVs) to achieve efficient conversion of the wide spectrum of sunlight into electricity. A remarkable improvement in power conversion efficiency (PCE) has been achieved through the use of innovative materials and device structures. However, a reliable technique for the rapid screening of the materials and processes is a prerequisite toward faster development in this area. Here we report the realization of such a versatile evaluation technique for bulk heterojunction OPVs by the combination of time-resolved microwave conductivity (TRMC) and submicrosecond white light pulse from a Xe-flash lamp. Xe-flash TRMC allows examination of the OPV active layer without requiring fabrication of the actual device. The transient photoconductivity maxima, involving information on generation efficiency, mobility, and lifetime of charge carriers in four well-known low band gap polymers blended with phenyl-C_{61}-butyric acid methyl ester (PCBM), were confirmed to universally correlate with the PCE divided by the open circuit voltage (PCE/V_{oc}), offering a facile way to predict photovoltaic performance without device fabrication.

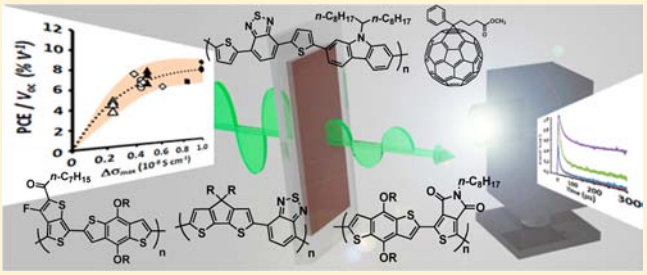

INTRODUCTION

Organic photovoltaics (OPV) have attracted special attention in applications that harvest the energy of sunlight, due to their material and manufacturing advantages.[1,2] Several innovations during the past decade have resulted in raising the power conversion efficiency (PCE) up to 10%.[3,4] Most of the research is directed toward the development of new device structures and novel materials.[5,6] The introduction of bulk heterojunction (BHJ) architecture[7,8] and the development of low band gap polymers[9,10] and soluble fullerene derivatives[11,12] have revolutionized this area. Several permutations such as the p/n blend ratio, solvents, solvent additives, and processing conditions could be optimized to realize the best efficiency from new materials; however, this can be a tedious procedure that has suppressed the rapid development of OPVs.

There have been only limited attempts toward achieving rapid development of OPVs using techniques that include transient absorption spectroscopy (TAS),[13,14] time-resolved terahertz spectroscopy (TRTS),[15,16] and time-resolved microwave conductivity (TRMC).[17−19] TAS gives only information about the time-evolutional concentration of transient species, while TRTS is limited to the femtosecond to nanosecond time domain and requires expensive laser systems and terahertz optics. Recently, we have reported the use of flash-photolysis TRMC to evaluate regioregular poly(3-hexylthiophene) (P3HT) and PCBM blend films, in which the transient photoconductivity was directly correlated with the PCE of the OPV device.[20] Therefore, this technique allows for the facile and stable evaluation of BHJ films without the need for device fabrication and is thus not subject to influences such as BHJ/metal interfacial issues, impurities, and degradation of the buffer and active layers.

Motivated by these results, we report a unique method of Xe-flash photolysis TRMC as a rapid and reliable evaluation scheme specific to the OPV characteristics of low band gap polymers. A BHJ film on a quartz substrate is exposed to a microsecond white light pulse (WLP) from a Xe-flash lamp, which gives rise to short-lived charge carriers. The time-resolved experiments revealed the key role of photocurrent generation and the resultant charge carrier dynamics of actual device performance. Comparison with conventional laser-flash TRMC verified that Xe-flash TRMC transients are universally correlated with PCE/V_{oc} for different p/n blend ratios of typical low band gap polymers. These results open the possibility to predict device performance without fabrication of the actual device structures and provide validation that this is a highly

Received: June 29, 2012
Published: November 13, 2012

   dx.doi.org/10.1021/ja309524f | J. Am. Chem. Soc. 2012, 134, 19035−19042

efficient tool for the evaluation of materials and processes toward the acceleration of OPV research.

RESULTS AND DISCUSSION

Development of Xe-Flash TRMC. Figure 1a shows the X-band (ca. 9.1 GHz) microwave circuit for TRMC experiments

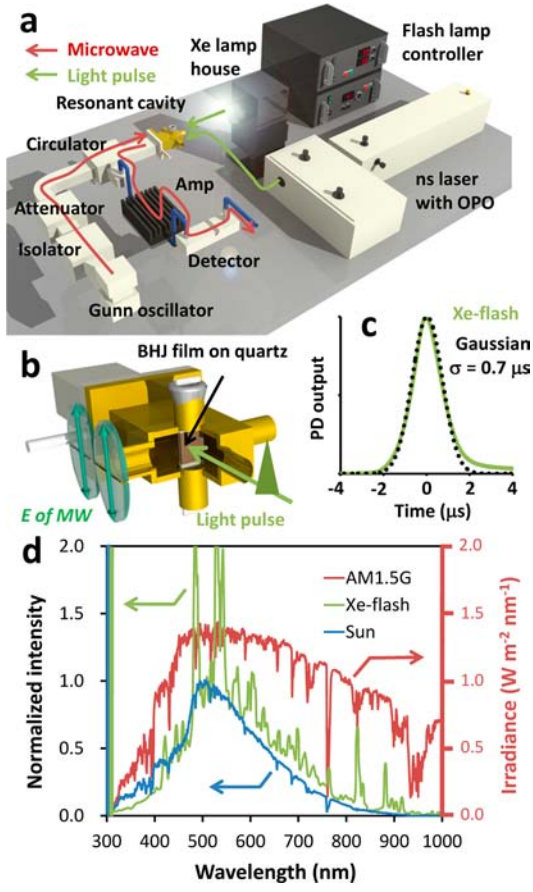

Figure 1. Schematic illustration of a Xe-flash TRMC measurement system. (a) Overall measurement system. The red and green arrows represent a stream of probing continuous microwaves in a microwave circuit and a pathway of excitation light pulses, respectively. (b) Resonant cavity with a BHJ film on a quartz substrate. The left front part is removed to expose the inside of the cavity. The substrate is set at the position of the front-side highest electric fields (E) of standing microwaves (MW). The excitation pulse is directed perpendicularly to the film. (c) Time profile of Xe-flash white light measured using a Si pin photodiode (PD, green). The black dotted line is a Gaussian fitting curve (σ = 0.70 μs, fwhm = 1.7 μs). (d) Solar spectrum of AM1.5G (red), white light spectrum from a Xe-flash lamp (green), and solar spectrum measured at Osaka, Japan on a fine day (blue). Note that the latter two spectra were measured using a spectrometer (sensitivity 300−1000 nm) without sensitivity calibration.

that was constructed according to our previous report.[17,21] A microwave resonant cavity with five pipes was adopted, where the vertical pair is used for sample loading and one horizontal pipe serves as a guide for the excitation light pulse (Figure 1b). A Xe-flash lamp was specially designed to meet the criteria for the TRMC experiment, such as high pulse energy, high repetition rate, small spot size, low electrical noise, and short pulse width. The temporal shape of the shortest WLP was well-fitted by a Gaussian function (Figure 1c), giving a standard deviation of 0.70 μs and a full-width at half-maximum (fwhm) of 1.7 μs. It should be noted that a submicro- to microsecond WLP was realized with relatively high energy (ca. 1 mJ pulse^{-1}) and high repetition rate (10 Hz), in contrast to the low energy of femtosecond WLP generated via nonlinear electrooptic effects[22,23] (on the order of nanojoules to microjoules per pulse, although the peak intensity per second is much higher than that of the Xe-flash WLP). Figure 1d presents white light spectra from the Xe-flash lamp, together with that for sunlight and an AM1.5G solar spectrum. Although Xe light has characteristic bright lines, the overall features match the sunlight spectrum of the reference, which indicates the possibility of direct use as pseudosolar light.

The time-resolution of the laser-flash TRMC system used in this study is 40−100 ns, which is dominated mainly by the Q-value of the resonant cavity rather than the laser pulse width (6 ns). On the contrary, the pulse width of the WLP (ca. 1−10 μs), which is much larger than the response time of a cavity, governs the overall time resolution of the Xe-flash TRMC system. At the sacrifice of a 2 orders of magnitude decrease in time resolution, the incident photon density for the Xe-flash (10^2−10^4 mJ cm^{-2} s^{-1}) becomes closer to that for 1 sun condition (100 mJ cm^{-2} s^{-1}) than the nanosecond laser-flash (10^5−10^8 mJ cm^{-2} s^{-1}). Moreover, the decrease in time-resolution demonstrates the unprecedented and positive effect for the photoconductivity analyses of BHJ films.

Relationship between Lifetime and Intensity of Transient Photoconductivity. Figure 2a presents kinetic decays of transient photoconductivity ($\Delta\sigma$) for a spin-coated P3HT:PCBM = 1:1 thin film obtained by laser-flash TRMC (λ_{ex} = 500 nm) and Xe-flash TRMC methods. Notably, the transient photoconductivity maximum ($\Delta\sigma_{max}$) of the latter is larger than the former, regardless of one order smaller light power of WLP (0.3 mJ cm^{-2} pulse^{-1}) than that of laser (2.5 mJ cm^{-2} pulse^{-1}). The transient signals obtained by WLP and laser pulse have a 2 orders of magnitude difference in the 10−90% rise times (4.5 μs and 64 ns, respectively), as well as the half-lifetimes, $\tau_{1/2}$ (11 and 0.55 μs, respectively). The decay rate is significantly dependent on the excitation photon density, in which the low laser power gives a low bulk charge recombination rate.[24,25] Therefore, the recombination speed is moderated for the low-photon density of WLP, which leads to an increase of long-lived charge carriers. We have reported that $\Delta\sigma_{max} \times \tau_{1/2}$ for the laser-flash TRMC transient decay has a good correlation with the short circuit current density J_{sc}, of P3HT:PCBM = 1:1 devices[20] and self-assembled semiconducting p/n nanotubes.[26,27] A long lifetime of TRMC transient means a low charge recombination rate and low probability of deactivation via trapping, leading to a high charge collection efficiency. Given the long-range charge carrier mobility of 10^{-4} cm^2 V^{-1} s^{-1}, as assessed from the space-charge limited current (SCLC)[28,29] and an active layer thickness of 100 nm, the time required for the charges to diffuse from the center to the counter electrode was calculated as 10 μs.[30] This time scale coincides with the rise time of the Xe-flash TRMC transient.

Accordingly we examined the relationship between lifetime and intensity of photoconductivity transients in the presence of response function. The observable decay, $c(t)$, is a convolution of a real function, $r(t)$, and a response function, $g(t)$, as expressed by

$$c(t) = \int_{-\infty}^{t} r(\tau)g(t-\tau)d\tau \quad (1)$$

dx.doi.org/10.1021/ja309524f | J. Am. Chem. Soc. 2012, 134, 19035−19042

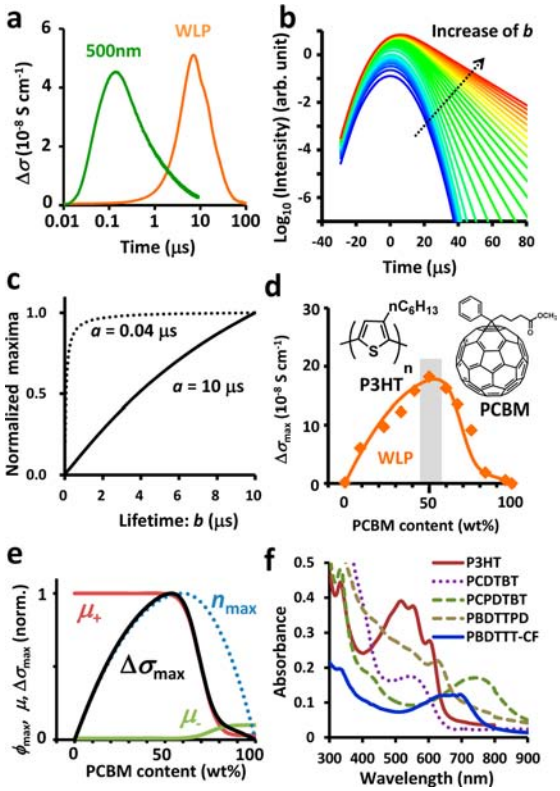

Figure 2. Photoconductivity of P3HT:PCBM films and photoabsorption spectrum of polymer:PCBM in the film state. (a) Transient photoconductivity of a spun-cast P3HT:PCBM = 1:1 film generated by laser-flash TRMC with 500 nm excitation (green line) and Xe-flash TRMC with WLP (orange line). (b) Single exponential decays convoluted by a 10 μs Gaussian response function assuming Xe-flash TRMC. The lifetime, b, was changed from 0.1 (blue) to 10 μs (red). See eqs 1−3. (c) Normalized maxima of convoluted exponential functions versus their lifetimes. The solid line (a = 10 μs) and dotted line (a = 0.04 μs) assumed the response times of Xe-flash and laser-flash TRMC, respectively. (d) Photoconductivity transient maxima ($\Delta\sigma_{max}$) versus p/n blend ratio in drop-cast P3HT:PCBM films induced by WLP. The chemical structures of P3HT and PCBM are shown in the inset. The orange solid line is a fitting curve. The gray belt indicates the best blend ratio for OPV device. (e) Component analysis of $\Delta\sigma_{max}$ dependence on the p/n blend ratio from panel d, where normalized curves of ϕ_{max} (dotted white blue line), μ_+ (red solid line), and μ_- (white green line, the amplitude is relative to μ_+) were assumed to reproduce the best fit of ϕ_{max} $(\mu_+ + \mu_-) \approx \Delta\sigma_{max}$ to the experiment. (f) Steady-state photoabsorption spectra of P3HT:PCBM = 1:1 (solid wine-red line), PCDTBT:PCBM = 1:4 (purple dots), PCPDTBT:PCBM = 1:3 (dashed green line), PBDTTPD:PCBM = 1:1.5 (brown dotted line), and PBDTTT-CF:PCBM = 1:1.5 (blue solid line) films.

For simplicity, we adopted a single exponential and Gaussian functions for $r(t)$ and $g(t)$, respectively, as given by

$$g(t) = \exp\left(-\frac{t^2}{a^2}\right) \quad (2)$$

$$r(t) = \exp\left(-\frac{t}{b}\right) \quad (3)$$

The convoluted decays based on eqs 1−3 with a = 10 μs assuming Xe-flash TRMC are displayed in Figure 2b (The Gaussian response function and exponential decays without convolution are shown in Supporting Figure S1). With an increase of exponential lifetime, b, the slope in the semi-logarithmic plot became milder, accompanied by an increase in the intensity maxima. The solid line in Figure 2c shows that the intensity maxima increase almost linearly with the lifetime, which demonstrates that $\Delta\sigma_{max}$ of Xe-flash TRMC includes not only mobility and density information but also the lifetime of charge carriers suitable for OPV characterization. In contrast, the intensity rapidly reaches saturation in the case of a = 0.04 μs (dotted line in Figure 2c, assuming laser-flash TRMC). In this case, the product of photoconductivity maxima and lifetime is a good indicator for correlating with J_{sc}.[20] However, an emphasis is given to that the charge carrier lifetime of laser-flash TRMC is also sensitive to the excitation photon density as discussed above, which iterates the unprecedented advantage of Xe-flash TRMC allowing a low excitation density experiments and inclusion of lifetime information into the maximum photoconductivity.

p/n Blend Ratio of P3HT:PCBM. The inclusion of charge carrier lifetime into the photoconductivity maxima of Xe-flash TRMC is strongly corroborated by the $\Delta\sigma_{max}$ dependence on the P3HT:PCBM blend ratio, as shown in Figure 2d. The largest $\Delta\sigma_{max}$ was obtained at P3HT:PCBM = 1:1, which is also the best blend ratio for maximum device performance. In contrast, the laser-flash TRMC with nanosecond time resolution has two $\Delta\sigma_{max}$ peaks at P3HT:PCBM = 1:1 and 1:40, which are due to hole- and electron-dominant conductivity, respectively ($\Delta\sigma_{max}$ and $\tau_{1/2}$ for various p/n composition observed in laser-flash TRMC is shown in Supporting Figure S2a).[20] The kinetic decay at 1:40 was much faster than that at 1:1, and thus $\Delta\sigma_{max} \times \tau_{1/2}$ displays one maximum at 1:1 (Supporting Figure S2b), as is the case with Xe-flash TRMC. The $\Delta\sigma_{max}$ is defined by $en_{max}(\mu_+ + \mu_-)$, where the parameters are the elementary charge (e), charge carrier density at the conductivity maximum (n_{max}), hole mobility (μ_+), and the electron mobility (μ_-). The solid line in Figure 2d was reproduced by assuming the dependence of n_{max}, μ_+, and μ_- on the p/n blend ratio, the components of which are presented in Figure 2e. For simplification of the analysis, error functions were adopted for μ_+ and μ_-, and a second-order curve for n_{max}. The error function-like curve has been reported for μ_+ of P3HT:perylenebisimide (PDI) blend films, where the incorporation of electron-accepting PDI leads to enhancement of the photoconductivity and determination of n_{max} by probing PDI radical anions via TAS.[31] The fluorescence from P3HT in P3HT:PCBM films is progressively quenched by electron transfer to PCBM, which leads to approximately 97% quenching, even in the presence of only 15 wt % PCBM.[7] However, $\Delta\sigma_{max}$ further increases with the PCBM content, which is understood by the formation of a long-range percolation network of PCBM domains that facilitate charge separation from the charge transfer (CT) state,[32] and this leads to a continuous increase of n_{max}. The second-order like curve has been reported in J_{sc} dependence on PCBM loading in regioregular poly(3-butylthiophene):PCBM film,[33] supporting our assumption. At a high PCBM content, the hole mobility abruptly decreases due to the collapse of intermolecular π stacking,[27,31] and instead, electron mobility becomes predominant. The relative values of μ_+ at P3HT = 100 wt % and μ_- at PCBM = 100 wt % are consistent with previous TRMC studies, i.e., 0.12−0.22 cm^2 V^{-1} s^{-1} for P3HT[20,31] and 0.04−0.3 cm^2 V^{-1} s^{-1} for PCBM.[34] Note that $\Delta\sigma_{max}$ for Xe-flash TRMC at a high PCBM content is further lowered, due to the fast

dx.doi.org/10.1021/ja309524f | J. Am. Chem. Soc. 2012, 134, 19035−19042

photoconductivity decay and subsequent decrease of the peak value.

p/n Blend Ratio of Low Band Gap Polymers. The following representative low band gap polymers were selected to examine the applicability of Xe-flash TRMC: poly[*N*-9″-hepta-decanyl-2,7-carbazole-alt-5,5-(4′,7′-di-2-thienyl-2′,1′,3′-benzothiadiazole)] (PCDTBT),[35−39] poly[2,6-(4,4-bis-(2-ethylhexyl)-4*H*-cyclopenta[2,1-*b*;3,4-*b*′]dithiophene)-alt-4,7(2,1,3-benzothiadiazole)] (PCPDTBT),[40−42] poly[2,6-(4,8-di(2-ethylhexyloxy)-benzo[1,2-*b*:4,5-*b*′]dithiophene)-alt-5-octyl-4*H*-thieno[3,4-*c*]pyrrole-4,6-dione] (PBDTTPD),[43−45] and poly-[4,8-bis-substituted-benzo[1,2-*b*:4,5-*b*′]dithiophene-2,6-diyl-alt-4-substituted-thieno[3,4b]thiophene-2,6-diyl] (PBDTTT-CF)[46] (analogous to PTB7),[36,47] all of which have exhibited high PCE. Steady-state photoabsorption spectra of the polymer films blended with typical PCBM concentrations are presented in Figure 2f. A variety of absorption spectra are evident, which emphasizes the advantages of WLP for precise evaluation. Figure 3 shows plots of $\Delta\sigma_{max}$ vs p/n blend ratio of these polymers measured by laser-flash TRMC with 355, 500, and 680 nm excitation (left panel) and Xe-flash TRMC (right panel). The overall photoconductivities of these low band gap polymers are small compared with P3HT:PCBM; however, in most cases of laser-flash TRMC, two distinct peaks appear at low and high PCBM contents. This is due to comparable or even smaller μ_+ compared to μ_- and a shift of the n_{max} peak toward a high PCBM content (Supporting Figure S3). For example, $\Delta\sigma_{max}$ by laser-flash TRMC for PCDTBT has two peaks for all excitation wavelengths, where the 680 nm excitation gave the most apparent first peak at PCDTBT:PCBM = 1:0.3 (Figure 3a). This wavelength lies on the longer-wavelength shoulder of the PCDTBT absorption spectrum maximum (Figure 2f), which corresponds to the most extended π-conjugation of the polymer backbone, and thus μ_+ of generated holes becomes larger than those generated in the amorphous region. Although the best p/n blend ratio of PCDTBT:PCBM has been reported as 1:4,[35−39] the peaks found by laser-flash TRMC are located at both 1:0.3 and 1:4, depending on the excitation wavelength. In contrast, Xe-flash TRMC clearly reveals a single peak at 1:4, as a result of convolutions of photoabsorption, charge separation efficiency, and the charge carrier mobility and lifetime, which enables direct and rapid optimization of the p/n blend ratio. The validity of Xe-flash TRMC was also confirmed for the other polymers, PCPDTBT, PBDTTPD, and PBDTTT-CF (Figures 3b−d).

Comparison with OPV Device Performance. The advantage of Xe-flash TRMC has motivates us to investigate more detailed correlations between photoconductivity and OPV device performance. Thin films of PCDTBT, PCPDTBT, PBDTTPD, and PBDTTT-CF blended with PCBM were prepared by spin-coating from *o*-dichlorobenzene (oDCB) or chlorobenzene (CB) solution with/without addition of a solvent processing additive (1,8-diiodooctane; DIO), similar to the procedure reported for device fabrication.[35−47] Figure 4a and b shows kinetic traces of the transient photoconductivity measured by laser-flash TRMC excited at 500 nm and Xe-flash TRMC, respectively. The PCE divided by V_{oc} reported for the respective polymers, process, and p/n blend ratios are plotted as a function of $\Delta\sigma_{max}$. The performance of these devices from the literature are listed in Supporting Table S1. Interestingly, PCE/V_{oc} is correlated with $\Delta\sigma_{max}$, even for laser-flash TRMC excited at 355 (Figure 4c), 500 (Figure 4d), and 680 nm

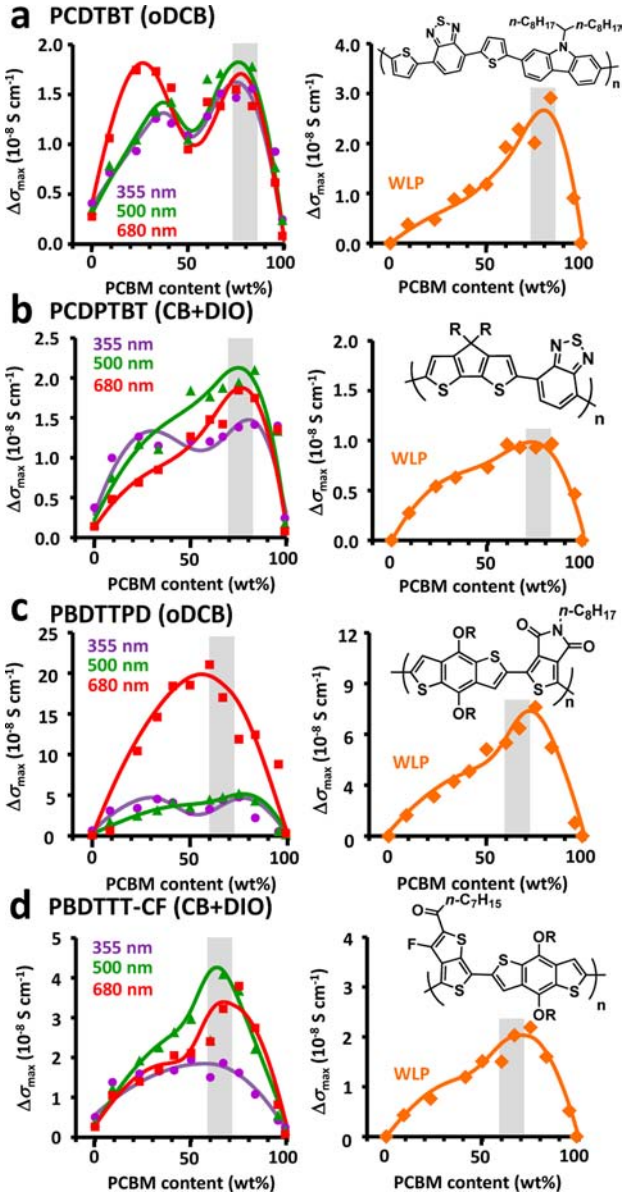

Figure 3. $\Delta\sigma_{max}$ vs p/n blend ratio investigated by laser- (left panel) and Xe-flash (right panel) TRMC. (a) PCDTBT:PCBM films drop-cast from oDCB solutions. (b) PCPDTBT:PCBM from CB solutions with 3% v/v DIO. (c) PBDTTPD:PCBM from oDCB solutions. (d) PBDTTT-CF:PCBM from CB solutions with 3% v/v DIO. The chemical structure of the low band gap polymer (R = 2-ethylhexyl) is displayed in the inset of each right panel. For the laser-flash TRMC, 355 (violet circles), 500 (green triangles), and 680 nm (red squares) were selected as excitation wavelengths. The solid colored lines were reproduced by assuming the dependence of ϕ_{max}, μ_+, and μ_- on the PCBM content (see Supporting Information). The gray bands represent the optimized p/n blend ratios in the reported OPV devices. Note that 50 wt % of PCBM is represented as polymer:PCBM = 1:1.

(Figure 4e); however, the deviation from an interpolated empirical double exponential function is large, in which the χ^2 parameters for fitting were 36.3, 16.1, 36.0, respectively. Excitation at 500 nm had better correlation for laser-flash TRMC, due to correspondence with the maximum irradiance in the solar spectrum (Figure 1d) as reported with respect to evaluation of the P3HT:PCBM system.[20] Nonetheless, as indicated by the gray arrows in Figure 4c−e, $\Delta\sigma_{max}$ of

dx.doi.org/10.1021/ja309524f | J. Am. Chem. Soc. 2012, 134, 19035−19042

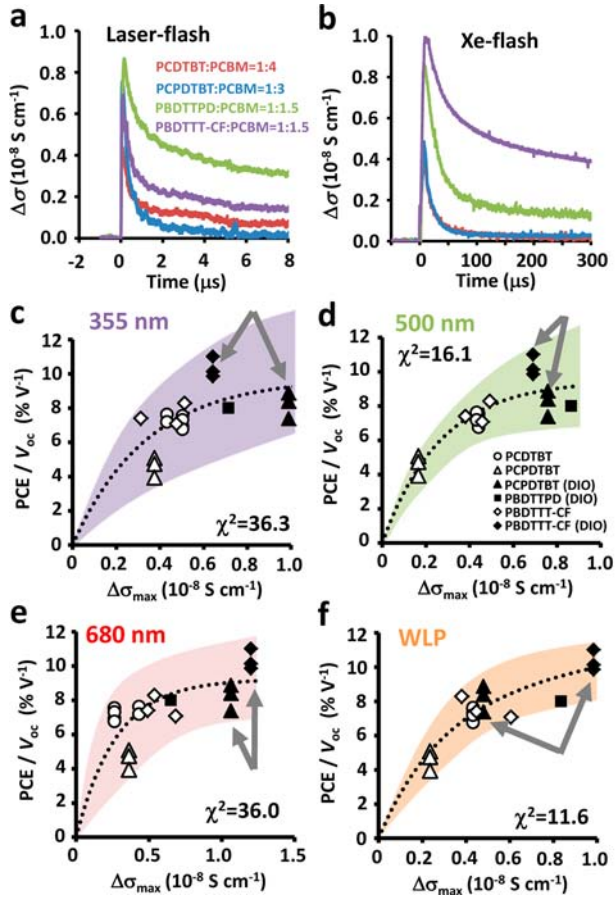

Figure 4. Correlation of $\Delta\sigma_{max}$ from TRMC photoconductivity transients and PCE/V_{oc} reported for OPV devices. Photoconductivity decay of polymer:PCBM blend films obtained by (a) laser-flash TRMC (excitation at 500 nm) and (b) Xe-flash TRMC. Correlation of PCE/V_{oc} and $\Delta\sigma_{max}$ is presented for laser-flash TRMC with excitation at (c) 355, (d) 500, and (e) 680 nm. (f) Xe-flash TRMC using WLP. Thin polymer:PCBM films (80−150 nm) at the best or close to the best blend ratios were prepared by spin-coating from optimized solutions, i.e., PCDTBT:PCBM = 1:4 from oDCB (open circles), PCPDTBT:PCBM = 1:3 from CB (open triangles), PCPDTBT:PCBM = 1:3 from CB with DIO (closed triangles), PBDTTPD:PCBM = 1:1.5 from CB with DIO (closed square), PBDTTT-CF:PCBM = 1:1, 1:1.5, and 1:2 from oDCB (open diamonds), and PBDTTT-CF:PCBM = 1:1.5 from CB with DIO (closed diamonds). The colored areas indicate the degree of divergent data plots. The dotted lines are double exponential functions obtained by least-squares fitting. The resultant χ^2 parameter is given in each panel. The gray arrows indicate PCPDTBT (DIO) and PBDTTT-CF(DIO) to emphasize the significant difference between the laser-flash TRMC and Xe-flash TRMC results.

PBDTTT-CF:PCBM = 1:1.5 film prepared from CB with DIO, which has demonstrated a significantly high PCE (e.g., 7.7%),[46] is lower than that for the PCPDTBT:PCBM = 1:3 film prepared from CB with DIO (PCE = 4.5−5.5%)[40−42] for 355 and 500 nm excitation, respectively. At 680 nm excitation, which is the absorption maximum of PBDTTT-CF, $\Delta\sigma_{max}$ of PBDTTT-CF became superior to that of PCPDTBT by approximately 13%. However, such a small change of $\Delta\sigma_{max}$, despite a large difference in PCE, along with the wavelength dependence makes it complicated to precisely evaluate the optoelectronic properties of the BHJ films. In contrast, such issues are circumvented by Xe-flash TRMC, as shown in Figure 4f, where PBDTTT-CF has the highest $\Delta\sigma_{max}$, and more importantly, its correlation with PCE/V_{oc} becomes more evident from the decrease in the χ^2 parameter to 11.6.

Excitation Intensity Dependence. To provide more insight into the charge carrier density and sublinear dependence observed in PCE/V_{oc} and $\Delta\sigma_{max}$, we examined excitation light intensity (P) dependence. Figure 5a presents $\Delta\sigma_{max}$ of Xe-flash

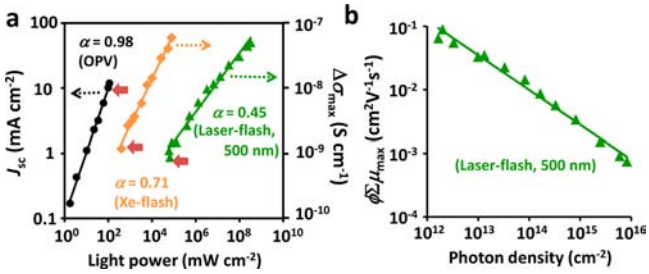

Figure 5. (a) Excitation intensity dependence of PBDTTT-CF:PCBM = 1:1.5 processed from chlorobenzene solution containing 3 % v/v DIO. The closed black circles represent a correlation between J_{sc} of the OPV device (left vertical axis) and intensity of continuous white light from a solar simulator. The orange diamonds and green triangles show the dependence of $\Delta\sigma_{max}$ (right vertical axis) on light intensities of a pulsed white light from a Xe-flash lamp and a 500 nm pulse from a nanosecond laser, respectively. Note that the energy density per pulse (mJ cm^{-2}) was divided by each pulse width (mJ cm^{-2} s^{-1} = mW cm^{-2}). The bold red arrows indicate the excitation light power that generates charge carrier density equivalent to 1 sun condition for each measurement. A drop-cast film was used for TRMC. The solid lines are the fitting curves given by eq 4, where α is an exponent. (b) $\phi\Sigma\mu_{max}$ dependence of PBDTTT-CF:PCBM = 1:1.5 film on incident photon density of laser-flash TRMC excited at 500 nm.

and laser-flash TRMC transients along with J_{sc} of the OPV device, where PBDTTT-CF:PCBM = 1:1.5 was processed from chlorobenzene solution containing DIO (all kinetic traces are shown in Supplementary Figure S4). The plots were fitted by the following equation:

$$\Delta\sigma_{max},\ J_{sc} \propto P^{\alpha} \quad (4)$$

where the exponent α is close to unity, which is an indication of weak bimolecular recombination.[25] In the OPV device, we found an almost linear relationship between J_{sc} and P (α = 0.98), which is in good agreement with the literatures.[24,25,36,48] In sharp contrast, Xe-flash and laser-flash TRMC indicated a sublinear dependence, giving α = 0.71 (Xe-flash) and 0.44 (laser-flash, 500 nm). This clearly shows that non-geminate bimolecular recombination loss is involved in both TRMC transients, which has been well-documented with transient absorption spectroscopy[30,49,50] and device characterization.[25,48] It is noteworthy that the loss is moderated in Xe-flash TRMC (larger α), due to the decrease in excitation photon density per second. This is consistent with a slightly straighter slope in the PCE/V_{oc} versus $\Delta\sigma_{max}$ plot of Xe-flash TRMC (Figure 4f) compared to that of laser-flash TRMC (Figure 4c−e).

The steady-state charge carrier generation rate calculated from J_{sc} under 1 sun illumination (Figure 5a) is on the order of 10^{21} cm^{-3} s^{-1},[25] which yields charge carrier density of 10^{16} cm^{-3} by assuming typical charge carrier mobility and active layer thickness.[30] In TRMC experiments using light pulse as an excitation, it is difficult to directly separate the charge carrier density (n_{max}) and the sum of mobility ($\Sigma\mu$) from the conductivity maxima ($\Delta\sigma_{max} = en_{max}\Sigma\mu$). Instead, inspecting

dx.doi.org/10.1021/ja309524f | J. Am. Chem. Soc. 2012, 134, 19035−19042

laser power dependence allows the estimation of the minimum charge carrier mobility, $\Sigma\mu_{min}$, because bimolecular recombination loss is suppressed and the charge carrier generation efficiency, ϕ (<1, see Experimental Section), is significantly increased at low laser intensity.[19,20,51] Figure 5b shows the $\phi\Sigma\mu$ peak value of the PBDTTT-CF:PCBM = 1:1.5 film as a function of incident laser photon density observed by laser-flash TRMC using 500 nm excitation. With a decrease of laser photon density (I_0), $\phi\Sigma\mu_{max}$ increased according to $I_0^{\alpha-1}$, where the α is the same value as in Figure 5a. The $\Sigma\mu_{min}$ of PBDTTT-CF:PCBM film was found to be 0.1 $cm^2\ V^{-1}\ s^{-1}$, which in turn leads to the charge carrier density of 10^{18} cm^{-3} at the laser and WLP power used through Figures 2−4. The carrier density is still 2 orders of magnitude higher than that of the short-circuit condition under 1 sun illumination, which pronounces again a key role of bulk recombination in the loss mechanism. The bold red arrows in Figure 5a indicate the excitation light power that generates charge carrier density equivalent to 1 sun condition for each measurement.

Discussion on Long- and Short-Range Mobilities. In addition to the difference in charge carrier concentration and resultant bulk recombination, the relationship between long-range charge carrier mobility assessed by direct-current technique such as SCLC (μ_{DC}) and short-range mobility probed by TRMC (μ_{TRMC})[52] would have some impact on the correlation between PCE/V_{oc} and $\Delta\sigma_{max}$. From the resonant soft X-ray scattering and grazing incidence wide-angle X-ray scattering experiments, Chen et al. claimed that a hierarchical nanomorphology in BHJ film plays a key role in exciton migration and its separation into charges, where polymer and PCBM crystallites are roughly phase-separated to form respectively rich domains surrounded by their amorphous phases.[53] TRMC can selectively probe the high charge carrier motion in the crystallites, while both intercrystallite and intracrystallite charge transport are responsible for μ_{DC}, in which the connection of crystallites is reasonably affected by the film preparation process, molecular weight, and crystallinity.[54,55] These factors reduce μ_{DC} and would cause the sublinear dependence given by $\mu_{TRMC} \approx \beta(\mu_{DC})^{\alpha}$, where the exponent α is less than unity and β is a coefficient. In the study of molecular weight dependence of P3HT film on TRMC and time-of-flight (TOF) mobilities,[55] α was estimated to be ca. 0.1. Investigations on fluorene-triphenylamine copolymers[52] or poly(carbazole)s[56] using TRMC and SCLC suggested that α is around 0.1−0.3. Meanwhile, a wide range of μ_{DC} values are reported for the low band copolymers, for example, PCDTBT hole mobilities varied by 3 orders of magnitude from 8.9×10^{-6} $cm^2\ V^{-1}\ s^{-1}$,[57] $1.5–9.6 \times 10^{-4}$ $cm^2\ V^{-1}\ s^{-1}$,[58] to 8×10^{-3} $cm^2\ V^{-1}\ s^{-1}$,[59] depending on measurement technique, solvent, annealing temperature, p/n blend ratio, and so on. Thus the correlation between μ_{TRMC} and μ_{DC} in BHJ film is still unclear and further investigation is required.

However, it is of particular interest to note that an upward trend between PCE/V_{oc} and $\Delta\sigma_{max}$ was found among the different types of low band gap polymers, their p/n blend ratios, and preparation processes (solvent and additive). Because PCE/V_{oc} is equivalent to J_{sc} × fill factor (*FF*), we separately plotted them as a function of $\Delta\sigma_{max}$ of Xe-flash TRMC (Figure 6). Interestingly, both J_{sc} and *FF* are roughly scaled with $\Delta\sigma_{max}$; however, the correlation became more scattered than their product (J_{sc} × *FF* = PCE/V_{oc}). This is probably due to that J_{sc} and *FF* are in a trade-off relationship, in terms of film thickness, photoabsorption, and charge carrier

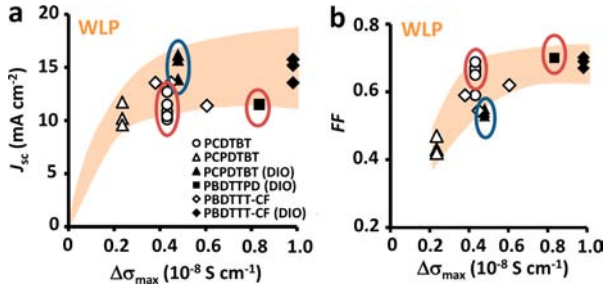

Figure 6. (a) J_{sc} and (b) *FF* plots versus $\Delta\sigma_{max}$ of Xe-flash TRMC using white light pulse (WLP). The product of J_{sc} and *FF* is equivalent to PCE/V_{oc} shown in Figure 4f. The blue and red ellipsoids represent data set of high J_{sc} and low *FF* and low J_{sc} and high *FF*, respectively.

mobility (transit time).[60] For example, PCDTBT and PBDTTPD enclosed by red ellipsoids show lower J_{sc} (Figure 6a) and higher *FF* (Figure 6b), while PCPDTBT(DIO) enclosed by blue ellipsoids indicate higher J_{sc} and lower *FF*. As a consequence, J_{sc} × *FF* becomes moderate and demonstrate a good correlation with $\Delta\sigma_{max}$. This allows for material and process screening without the need for OPV devices fabrication. Thus, the PCE/V_{oc} of a new polymer could be predicted by measuring $\Delta\sigma_{max}$ of the blend thin film, based on the accumulated data of Xe-flash TRMC for optimized and successful examples.

The wide-covering photoabsorption properties of low band gap polymers with low HOMO levels has realized increasing PCEs over the past several years. For example, the highly crystalline properties like those of P3HT, which demonstrates high external quantum efficiency in its photoabsorption regime, are anticipated to also be incorporated as a low band gap polymer. The P3HT:PCBM thin film has $\Delta\sigma_{max}$ from Xe-flash TRMC that is approximately 5 times larger than those of examined low band gap polymers. The highest PCE/V_{oc} of P3HT:PCBM is 8.1 (PCE = 5.2%).[61] We should emphasize that P3HT:PCBM has an exceptionally high $\Delta\sigma_{max}$ due to its highly crystalline nature. This is the case given that the dependence of PCE/V_{oc} on $\Delta\sigma_{max}$ is different from the low band gap polymers. Although selection of a polymer backbone with high charge carrier mobility is a typical approach to realize high performance OPV,[62] the correlation between mobility and PCE is still vague.[63] Further investigation could clarify the fundamental aspects that hamper current efficient extraction in OPV devices.

■ CONCLUSION

Xe-flash TRMC using WLP with a pseudosolar spectrum was developed as a versatile platform for the facile screening of materials and processes. The photon density (10^2−10^4 mJ cm^{-2} s^{-1}) and pulse width of the WLP (ca. 10 μs) were confirmed as suitable for this purpose, which allows for direct correlation of the transient photoconductivity maxima with the PCE/V_{oc} of BHJ devices consisting of low band gap polymers. Investigation of the p/n blend ratio of these polymers to methanofullerene highlighted the advantage of Xe-flash TRMC over laser-flash TRMC, where the former gave a single peak close to the optimized blend ratio found in actual devices. Thus, Xe-flash TRMC can predict photovoltaic performance without the need for device fabrication, which should facilitate the rapid development of OPV devices.

dx.doi.org/10.1021/ja309524f | J. Am. Chem. Soc. 2012, 134, 19035−19042

EXPERIMENTAL SECTION

General. Steady-state photoabsorption spectroscopy was performed using a Jasco V-570 UV−vis spectrophotometer. Solar spectrum and white light spectrum from a Xe-flash lamp were measured through an optical fiber using an Ocean Optics HR4000 spectrometer. Note that the sensitivity is limited from 300 to 1000 nm, the output intensity of which is not calibrated. The time profile of the WLP from a Xe-flash lamp was measured using a Si pin photodiode (Hamamatsu Inc. S1722-22).

Materials. PCBM (purity >99.5%) was obtained from Frontier Carbon Inc. PBDTTT-CF was purchased from One-Material Inc. PCDTBT, PCPDTBT, and PBDTTPD were synthesized in accordance with previous reports,[34−46] the details of which are given in the Supporting Information. Solvents were purchased from Kishida Kagaku Corp. unless otherwise noted and were used as-received without further purification.

Time-Resolved Microwave Conductivity (TRMC). A resonant cavity was used to obtain a high degree of sensitivity in the conductivity measurement. The resonant frequency and microwave power were set at ca. 9.1 GHz and 3 mW, respectively, so that the electric field of the microwave was sufficiently small to not disturb the motion of charge carriers. The third harmonic generation (THG; 355 nm) of a Nd:YAG laser (Continuum Inc., Surelite II, 5−8 ns pulse duration, 10 Hz) or 500 and 680 nm pulses from an optical parametric oscillator (Continuum Inc., Panther) seeded by THG of a Nd:YAG laser were used as an excitation source. The laser power was fixed at 2.5 mJ cm^{-2} $pulse^{-1}$ for all excitation wavelengths (incident photon density, I_0 = 4.6, 6.4, and 8.7 × 10^{15} photons cm^{-2} $pulse^{-1}$ for 355, 500, and 680 nm, respectively). An in-house-built Xe-flash lamp (10 μs pulse duration, 10 Hz) with a power of 0.3 mJ cm^{-2} $pulse^{-1}$ was used for the Xe-flash TRMC experiments. For the attenuation of excitation light energy, neutral density filters were used for both Xe-flash and laser-flash TRMC. In the case of laser-flash TRMC, the photoconductivity transient $\Delta\sigma$ is converted to the product of the quantum efficiency: ϕ and the sum of charge carrier mobilities, $\Sigma\mu$, by $\phi\Sigma\mu = \Delta\sigma\ (eI_0F_{light})^{-1}$, where e and F_{Light} are the unit charge of a single electron and a correction (or filling) factor.

Organic Photovoltaic Cell (OPV). A PEDOT:PSS layer was cast onto the cleaned ITO layer by spin-coating after passing through a 0.2 μm filter. The substrate was annealed on a hot plate at 150 °C for 30 min. A 1 wt % chlorobenzene solution of PBDTTT-CF:PCBM = 1:1.5 w/w with 3% v/v 1,8-diiodeoctane (DIO) were cast on top of the PEDOT:PSS buffer layer in a nitrogen glovebox by spin-coating after passing through a 0.2 μm filter. A cathode consisting of 20 nm Ca and 100 nm Al layers was sequentially deposited through a shadow mask on top of the active layers by thermal evaporation in a vacuum chamber. The resulting device configuration was ITO (120−160 nm)/PEDOT:PSS (45−60 nm)/active layer (ca. 100 nm)/Ca (20 nm)/Al (100 nm) with an active area of 7.1 mm^2. Current−voltage (J−V) curves were measured using a source-measure unit (ADCMT Corp., 6241A) under AM 1.5 G solar illumination at 100 mW cm^{-2} (1 sun) using a 300 W solar simulator (SAN-EI Corp., XES-301S).

ASSOCIATED CONTENT

Supporting Information

Synthesis of the monomers and polymers and Supporting Figures S1−S4. This material is available free of charge via the Internet at http://pubs.acs.org.

AUTHOR INFORMATION

Corresponding Author

saeki@chem.eng.osaka-u.ac.jp

Notes

The authors declare no competing financial interest.

ACKNOWLEDGMENTS

This work was supported by the Precursory Research for Embryonic Science and Technology (PRESTO) program of the Japan Science and Technology Agency (JST), Tenure Track Program at the Frontier Research Base for Global Young Researchers of JST and Osaka University, and a KAKENHI grant from the Ministry of Education, Culture, Sports, Science and Technology (MEXT) of Japan.

REFERENCES

(1) Hardin, B. E.; Snaith, H. J.; McGehee, M. D. *Nat. Photonics* **2012**, *6*, 162−169.
(2) Li, G.; Zhu, R.; Yang, Y. *Nat. Photonics* **2012**, *6*, 153−161.
(3) Service, R. F. *Science* **2011**, *332*, 293−293.
(4) Green, M. A.; Emery, K.; Hishikawa, Y.; Warta, W.; Dunlop, E. D. *Prog. Photovoltaics* **2012**, *20*, 12−20.
(5) Gendron, D.; Leclerc, M. *Energy Environ. Sci.* **2011**, *4*, 1225−1237.
(6) Beaujuge, P. M.; Fréchet, J. M. J. *J. Am. Chem. Soc.* **2011**, *133*, 20009−20029.
(7) Yu, G.; Gao, J.; Hummelen, J. C.; Wudl, F.; Heeger, A. J. *Science* **1995**, *270*, 1789−1791.
(8) Peet, J.; Heeger, A. J.; Bazan, G. C. *Acc. Chem. Res.* **2009**, *42*, 1700−1708.
(9) Sun, Y.; Welch, G. C.; Leong, W. L.; Takacs, C. J.; Bazan, G. C.; Heeger, A. J. *Nat. Mater.* **2012**, *11*, 44−48.
(10) Brédas, J. −L.; Norton, J. E.; Cornil, J.; Coropceanu, V. *Acc. Chem. Res.* **2009**, *42*, 1691−1699.
(11) Matsuo, Y.; Sato, Y.; Niinomi, T.; Soga, I.; Tanaka, H.; Nakamura, E. *J. Am. Chem. Soc.* **2009**, *131*, 16048−16050.
(12) Zhao, G.; He, Y.; Li, Y. *Adv. Mater.* **2010**, *22*, 4355−4358.
(13) Clarke, T. M.; Durrant, J. R. *Chem. Rev.* **2010**, *110*, 6736−6767.
(14) Baranovskii, S. D.; Wiemer, M.; Nenashev, A. V.; Jansson, F.; Gebhard, F. *J. Phys. Chem. Lett.* **2012**, *3*, 1214−1221.
(15) Bartelt, A. F.; Strothkämper, C.; Schindler, W.; Fostiropoulos, K.; Eichberger, R. *Appl. Phys. Lett.* **2011**, *99*, 143304/1−3.
(16) Cooke, D. G.; Krebs, F. C.; Jepsen, P. U. *Phys. Rev. Lett.* **2012**, *108*, 056603/1−5.
(17) Saeki, A.; Koizumi, Y.; Aida, T.; Seki, S. *Acc. Chem. Res.* **2012**, *45*, 1193−1202.
(18) Grozema, F. C.; Siebbeles, L. D. A. *J. Phys. Chem. Lett.* **2011**, *2*, 2951−2958.
(19) Rance, W. L.; Ferguson, A. J.; McCarthy-Ward, T.; Heeney, M.; Ginley, D. S.; Olson, D. C.; Rumbles, G.; Kopidakis, N. *ACS Nano* **2011**, *5*, 5635−5646.
(20) Saeki, A.; Tsuji, M.; Seki, S. *Adv. Energy Mater.* **2011**, *1*, 661−669.
(21) Saeki, A.; Seki, S.; Sunagawa, T.; Ushida, K.; Tagawa, S. *Philos. Mag.* **2006**, *86*, 1261−1276.
(22) Ghotbi, M.; Petrov, V.; Noack, F. *Opt. Lett.* **2010**, *35*, 2139−2141.
(23) Dharmadhikari, A. K.; Rajgara, F. A.; Mathur, D. *Appl. Phys. B: Lasers Opt.* **2005**, *80*, 61−66.
(24) Maurano, A.; Hamilton, R.; Shuttle, C. G.; Ballantyne, A. M.; Nelson, J.; O'Regan, B.; Zhang, W.; McCulloch, I.; Azimi, H.; Morana, M.; Brabec, C. J.; Durrant, J. R. *Adv. Mater.* **2010**, *22*, 4987−4992.
(25) Koster, L. J. A.; Kemerink, M.; Wienk, M. M.; Maturová, K.; Janssen, R. A. J. *Adv. Mater.* **2011**, *23*, 1670−1674.
(26) Yamamoto, Y.; Zhang, G.; Jin, W.; Fukushima, T.; Ishii, N.; Saeki, A.; Seki, S.; Tagawa, S.; Minari, T.; Tsukagoshi, K.; Aida, T. *Proc. Natl. Acad. Sci. U.S.A.* **2009**, *106*, 21051−21056.
(27) Saeki, A.; Yamamoto, Y.; Koizumi, Y.; Fukushima, T.; Aida, T.; Seki, S. *J. Phys. Chem. Lett.* **2011**, *2*, 2549−2554.
(28) Mihailetchi, V. D.; Xie, H.; de Boer, B.; Koster, L. J. A.; Blom, P. W. M. *Adv. Funct. Mater.* **2006**, *16*, 699−708.
(29) Son, H. J.; Wang, W.; Xu, T.; Liang, Y.; Wu, Y.; Li, G.; Yu, L. *J. Am. Chem. Soc.* **2011**, *133*, 1885−1894.

(30) Guo, J.; Ohkita, H.; Yokoya, S.; Benten, H.; Ito, S. *J. Am. Chem. Soc.* **2010**, *132*, 9631−9637.
(31) Saeki, A.; Ohsaki, S.-i.; Seki, S.; Tagawa, S. *J. Phys. Chem. C* **2008**, *112*, 16643−16650.
(32) Bakulin, A. A.; Rao, A.; Pavelyev, V. G.; van Loosdrecht, P. H. M.; Pshenichnikov, M. S.; Niedzialek, D.; Cornil, J.; Beljonne, D.; Friend, R. H. *Science* **2012**, *335*, 1340−1344.
(33) Xin, H.; Ren, G.; Kim, F. S.; Jenekhe, S. A. *Chem. Mater.* **2008**, *20*, 6199−6207.
(34) de Haas, M. P.; Warman, J. M.; Anthopoulos, T. D.; de Leeuw, D. M. *Adv. Funct. Mater.* **2006**, *16*, 2274−2280.
(35) Park, S. H.; Roy, A.; Beaupré, S.; Cho, S.; Coates, N.; Moon, J. S.; Moses, D.; Leclerc, M.; Lee, K.; Heeger, A. J. *Nat. Photonics* **2009**, *3*, 297−303.
(36) He, Z.; Zhong, C.; Huang, X.; Wong, W.-Y.; Wu, H.; Chen, L.; Su, S.; Cao, Y. *Adv. Mater.* **2011**, *23*, 4636−4643.
(37) Sun, Y.; Takacs, C. J.; Cowan, S. R.; Seo, J. H.; Gong, X.; Roy, A.; Heeger, A. J. *Adv. Mater.* **2011**, *23*, 2226−2230.
(38) Steirer, K. X.; Ndione, P. F.; Widjonarko, N. E.; Lloyd, M. T.; Meyer, J.; Ratcliff, E. L.; Kahn, A.; Armstrong, N. R.; Curtis, C. J.; Ginley, D. S.; Berry, J. J.; Olson, D. C. *Adv. Energy Mater.* **2011**, *1*, 813−820.
(39) Sun, Y.; Seo, J. H.; Takacs, C. L.; Seifter, J.; Heeger, A. J. *Adv. Mater.* **2011**, *23*, 1679−1683.
(40) Lee, J. K; Ma, W. L.; Brabec, C. J.; Yuen, J.; Moon, J. S.; Kim, J. Y.; Lee, K.; Bazan, G. C.; Heeger, A. J. *J. Am. Chem. Soc.* **2008**, *130*, 3619−3623.
(41) Peet, J.; Kim, J. Y.; Coates, N. E.; Ma, W. L.; Moses, D.; Heeger, A. J.; Bazan, G. C. *Nat. Mater.* **2007**, *6*, 497−500.
(42) Albrecht, S.; Schindler, W.; Kurpiers, J.; Kniepert, J.; Blakesley, J. C.; Dumsch, I.; Allard, S.; Fostiropoulos, K.; Scherf, U.; Neher, D. *J. Phys. Chem. Lett.* **2012**, *3*, 640−645.
(43) Piliego, C.; Holcombe, T. W.; Douglas, J. D.; Woo, C. H.; Beaujuge, P. M.; Fréchet, J. M. J. *J. Am. Chem. Soc.* **2010**, *132*, 7595−7597.
(44) Zou, Y.; Najari, A.; Berrouard, P.; Beaupré, S.; Aïch, B. R.; Tao, Y.; Leclerc, M. *J. Am. Chem. Soc.* **2010**, *132*, 5330−5331.
(45) Zhang, Y.; Hau, S. K.; Yip, H.-L.; Sun, Y.; Acton, O.; Jen, A. K.-Y. *Chem. Mater.* **2010**, *22*, 2696−2698.
(46) Chen, H. −Y.; Hou, J.; Zhang, S.; Liang, Y.; Yang, G.; Yang, Y.; Yu, L.; Wu, Y.; Li, G. *Nat. Photonics* **2009**, *3*, 649−653.
(47) Liang, Y.; Xu, Z.; Xia, J.; Tsai, S.-T.; Wu, Y.; Li, G.; Ray, C.; Yu, L. *Adv. Mater.* **2010**, *22*, E135−E138.
(48) Koster, L. J. A.; Mihailetchi, V. D.; Xie, H.; Blom, P. W. M. *Appl. Phys. Lett.* **2005**, *87*, 203502/1−3.
(49) Clarke, T. M.; Jamieson, F. C.; Durrant, J. R. *J. Phys. Chem. C* **2009**, *113*, 20934−20941.
(50) Etzold, R.; Howard, I. A.; Mauer, R.; Meister, M.; Kim, T. −D.; Lee, K. −S.; Baek, N. S.; Laquai, F. *J. Am. Chem. Soc.* **2011**, *133*, 9469−9479.
(51) Savenije, T. J.; Kroeze, J. E.; Yang, X.; Loos, J. *Adv. Funct. Mater.* **2005**, *15*, 1260−1266.
(52) Fukumatsu, T.; Saeki, A.; Seki, S. *Appl. Phys. Express* **2012**, *5*, 061701/1−3.
(53) Chen, W.; Xu, T.; He, F.; Wang, W.; Wang, C.; Strzalka, J.; Liu, Y.; Wen, J.; Miller, D. J.; Chen, J.; Hong, K.; Yu, L.; Darling, S. B. *Nano Lett.* **2011**, *11*, 3707−3713.
(54) Hiorns, R. C.; de Bettignies, R.; Leroy, J.; Bailly, S.; Firon, M.; Sentein, C.; Khoukh, A.; Preud'homme, H.; Dagron-Lartigau, C. *Adv. Funct. Mater.* **2006**, *16*, 2263−2273.
(55) Pingel, P.; Zen, A.; Abellón, R. D.; Grozema, F. C.; Siebbeles, L. D. A.; Neher, D. *Adv. Funct. Mater.* **2010**, *20*, 2286−2295.
(56) Yasutani, Y.; Honsho, Y.; Saeki, A.; Seki, S. *Synth. Met.* **2012**, *162*, 1713−1721.
(57) Chan, K. K. H.; Tsang, S. W.; Lee, H. K. H.; So, F.; So, S. K. *Org. Electron.* **2012**, *13*, 850−855.
(58) Chu, T.-Y.; Alem, S.; Tsang, S.-W.; Tse, S.-C.; Wakim, S.; Lu, J.; Dennler, G.; Waller, D.; Gaudiana, R.; Tao, Y. *Appl. Phys. Lett.* **2011**, *98*, 253301/1−3.
(59) Cowan, S. R.; Street, R. A.; Cho, S.; Heeger, A. J. *Phys. Rev. B* **2011**, *83*, 035205/1−8.
(60) Ayzner, A. L.; Tassone, C. J.; Tolbert, S. H.; Schwartz, B. J. *J. Phys. Chem. C* **2009**, *113*, 20050−20060.
(61) Irwin, M. D.; Buchholz, D. B.; Hains, A. W.; Chang, R. P. H.; Marks, T. J. *Proc. Natl. Acad. Sci. U.S.A.* **2008**, *105*, 2783−2787.
(62) Osaka, I.; Abe, T.; Shimawaki, M.; Koganezawa, T.; Takimiya, K. *ACS Macro Lett.* **2012**, *1*, 437−440.
(63) Lecover, R.; Williams, N.; Markovic, N.; Reich, D. H.; Naiman, D. Q.; Katz, H. E. *ACS Nano* **2012**, *6*, 2865−2870.